Proceedings of the Sixteenth International Conference on
Computational Structures Technology
Edited by: P. Iványi, J. Kruis and B.H.V. Topping
Civil-Comp Conferences, Volume 14, Paper 15.3
Civil-Comp Press, Edinburgh, United Kingdom, 2026
ISSN: 2753-3239, doi: 10.4203/ccc.14.15.3

Application of Hierarchical Rotational Shell Finite Elements

I. Páczelt[1], B. Szabó[2] and A. Baksa[1]

[1]Institute of Applied Mechanics, University of Miskolc, Hungary
[2]Washington University in St. Louis, USA

Abstract

This paper provides a concise overview of the structure of hierarchical shell finite elements and presents computational results for various rotational shell structures. The numerical examples convincingly demonstrate that convergent solutions can be achieved by employing a sufficient number of hierarchical levels. In these elements, higher-order polynomials (*director functions*) are used in the direction perpendicular to the centerline, while conventional p-version shape functions (*field functions*) are applied along the centerline. The displacement field is represented as a sum of products of the director and field functions. By varying the number of director functions, different hierarchical levels of approximation are obtained. With appropriate mesh design and the combined use of the p-version, exponential convergence rates can be achieved. Furthermore, convergence surfaces enable the identification of the minimum hierarchical level required to obtain an accurate solution.

Keywords: finite element method, hierarchical model, shells of revolution, theory of elasticity, convergence solutions, director and field functions

1 Introduction

In engineering practice, a key objective when formulating mechanical models is to balance computational efficiency with physical fidelity. That is, one seeks models

with a limited number of unknowns and low computational cost while still capturing the essential characteristics of real structural behavior. For thin-walled bodies, this objective can be achieved through dimensional reduction: instead of modeling all three spatial coordinates, one or two coordinates are used, as is common in beam, plate, and shell theories.
For beam modeling, the Euler–Bernoulli hypothesis [1] or the Timoshenko theory [2] is most commonly used. In the case of plates and shells, the commonly used assumptions include the Kirchhoff–Love [3,7], Reissner–Mindlin [4,5], and Naghdi [6] hypotheses. Models with higher-order kinematic approximations have also been developed, such as Reddy’s cubic plate theory [8].
The goals of model development are very different today from those in the classical period. In the classical period, the goal was to formulate plate and shell problems so that they could be treated by classical methods—that is, finding analytic solutions to the governing partial differential equations. Today, the goal is to control model-form errors using hierarchical sequences of models [9,10].
In these formulations, higher-order polynomials—called *director functions*—are employed in the direction perpendicular to the centerline or midsurface, while mapped polynomials constructed from hierarchic shape functions (*field functions*) are used on the centerline or surface. By varying the number of director functions included in the approximation, a sequence of nested models are obtained.
Many engineering applications involve shells with axisymmetric geometry and loading conditions. The present study focuses on the development of hierarchical models for this class of shells.
In our previous work, hierarchical models based on p-version finite elements were developed for spatial beam structures composed of linear elastic materials [11]. Within the framework of linear elasticity, these models were derived from the principle of minimum potential energy, with the displacement field approximated as the product of functions describing the cross-sectional and longitudinal distributions:

$$\mathbf{u} = \mathbf{u}(x, y, s) = \mathbf{U}(x, y)\boldsymbol{\psi}(s) = \mathbf{U}(x, y)\left\{\mathbf{G}(s)\mathbf{q} + \boldsymbol{\Phi}(s)\mathbf{a}\right\} \tag{1}$$

where $\mathbf{U}(x,y)$ is the matrix containing power functions (the director functions) ordered according to Pascal's triangle, $\boldsymbol{\psi}(s)$ is the vector containing field functions approximated usin the p-version of the finite element method. Here, (x,y,s) denotes the curvilinear coordinate system: the x and y axes coincide with the main axes of the cross section, and s is the arc length measured along the centerline, $\mathbf{G}(s)$, $\boldsymbol{\Phi}(s)$ are the approximation matrices, $\mathbf{q}$ is the generalized nodal displacement vector, and $\mathbf{a}$ is the vector of additional coefficients. Depending on the number of polynomials included in $\mathbf{U}(x, y)$, a model with different hierarchies can be formed. Regarding beam structures, the work [12] deals with classical and higher-level theories. Additional references can be found in [11]. Particular emphasis should be placed on works [13,14] concerning shells and plates. The general principles of hierarchical modeling are presented in [15].

2 Construction of curved finite elements

In p-version finite element formulations, precise mapping of the geometry of the modeled bodies is of critical importance. We investigate a finite element defined along the meridian of a rotationally symmetric body, illustrated in Figure 1, with its first and third sides being circular. The radii of the circles are r_{1-2} and r_{4-3}. With the following notations: $\alpha_k = (\alpha_{1-4} + \alpha_{2-3})/2, \alpha_d = (\alpha_{1-4} - \alpha_{2-3})/2$, the mapping between the local curvilinear ξ,ζ and the global coordinate system r,z is as follows [10]:

$$r = (r_{1-2}\frac{1-\zeta}{2} + r_{4-3}\frac{1+\zeta}{2})\cos(\alpha_k - \xi\alpha_d),\ z\ = (r_{1-2}\frac{1-\zeta}{2} + r_{4-3}\frac{1+\zeta}{2})\sin(\alpha_k - \xi\alpha_d) \quad (2)$$

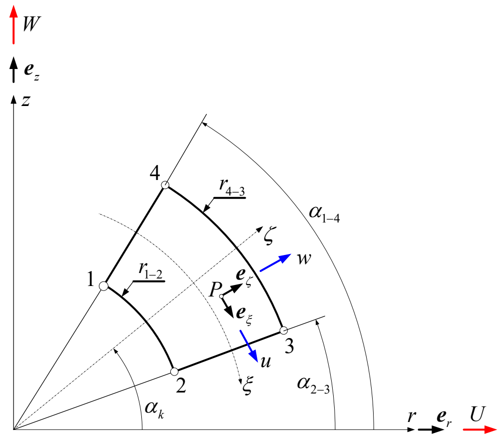

Figure 1: Shell element, a) mapping and displacements, b) shell finite element between *IJ* nodes

The displacement in the local coordinate system is approximated in the following form:

$$\mathbf{u}_L = u\mathbf{e}_\xi + w\mathbf{e}_\zeta \Rightarrow \mathbf{u}_L = \begin{bmatrix} u \\ w \end{bmatrix} = \sum_{m=1}^{MM} \mathbf{U}_m(\xi) F_m(\zeta)\,, \quad (3)$$

where $\mathbf{U}_m(\xi)$ contains the usual shape functions. The term $F_m(\zeta) = (\zeta)^{m-1}$ represents the distribution of the displacement along the thickness of the shell (for convenient reference, the function $F_m(\zeta)$ is briefly characterized by the following notation and value: ipolt=1). In our calculations, we also use the Legendre polynomials (ipolt=0), or their combination, the so-called $\Phi(\zeta)$ functions (ipolt= -1) [10]. Depending on the choice of *MM*, hierarchical models of different levels are obtained; that is, the resulting models can reproduce or even exceed the predictive capabilities of various shell and plate theories. The parameter *MM* determines the degree of the polynomial used to approximate the variation through the thickness.

At $MM = 2$ we perform the calculation according to the conditions of Naghdi's shell theory. Let

$$N_1 = 0.5(1-\xi) = N_I, \quad N_2 = 0.5(1+\xi) = N_J,$$
$$N_{p+1} = (0.5(1+\xi))^p - 0.5(1+\xi),\ p = 2,3,...,np \ ,$$
$$\mathbf{N}_I = \begin{bmatrix} N_I & 0 \\ 0 & N_I \end{bmatrix}, I \to J, \hat{\mathbf{N}}_{p-1} = \begin{bmatrix} N_{p+1} & 0 \\ 0 & N_{p+1} \end{bmatrix}, p = 2,3,...,np \ , \tag{4}$$

where np is the highest power of the approximating polynomial. Then, instead of Equation (3), we can write the approximation in terms of nodal displacements and additional constants. Denote the nodes of the element by I, J (see Fig. 1b). Thus, the displacement in the local system of the finite element is

$$\mathbf{u}_L = u\mathbf{e}_\xi + w\mathbf{e}_\zeta \Rightarrow \mathbf{u}_L = \begin{bmatrix} u \\ w \end{bmatrix} = \sum_{m=1}^{MM} \mathbf{U}_m(\xi) F_m(\zeta) = \sum_{m=1}^{MM} F_m \left\{ \begin{bmatrix} \mathbf{N}_I & \mathbf{N}_J \end{bmatrix} \begin{bmatrix} \mathbf{q}_I^m \\ \mathbf{q}_J^m \end{bmatrix} + \sum_{j=1}^{np-1} \hat{\mathbf{N}}_j \hat{\mathbf{a}}_j^m \right\}$$
$$= \sum_{m=1}^{MM} \left\{ \begin{bmatrix} \mathbf{G}_I^m & \mathbf{G}_J^m \end{bmatrix} \begin{bmatrix} \mathbf{q}_I^m \\ \mathbf{q}_J^m \end{bmatrix} + \begin{bmatrix} \hat{\mathbf{G}}_1^m & \hat{\mathbf{G}}_2^m, ..., \hat{\mathbf{G}}_{np-1}^m \end{bmatrix} \begin{bmatrix} \hat{\mathbf{a}}_1^m \\ \hat{\mathbf{a}}_2^m \\ \cdot \\ \hat{\mathbf{a}}_{np-1} \end{bmatrix} \right\}$$

Replacing the summation with matrix multiplications, the total displacement in the local coordinate system of the examined finite element is

$$\mathbf{u}_L = \mathbf{u}_L(\xi,\zeta) = \Big[\underset{(2,2MM)}{\mathbf{G}_I^L(\xi,\zeta)} \ \underset{(2,2MM)}{\mathbf{G}_J^L(\xi,\zeta)} \Big] \underset{(4MM,1)}{\begin{bmatrix} \mathbf{q}_I^L \\ \mathbf{q}_J^L \end{bmatrix}} + \underset{(2,2(np-1)MM)}{\hat{\mathbf{G}}(\xi,\zeta)} \ \underset{(2(np-1)MM,1)}{\hat{\mathbf{a}}} ,$$

$$\mathbf{u}_L = \mathbf{u}_L(\xi,\zeta) = \underset{(2,4MM)}{\mathbf{G}^L(\xi,\zeta)} \ \underset{(4MM,1)}{\mathbf{q}^L} + \underset{(2,2(np-1)MM)}{\hat{\mathbf{G}}(\xi,\zeta)} \ \underset{(2(np-1)MM,1)}{\hat{\mathbf{a}}} , \tag{5}$$

where

$$\mathbf{G}^L = \mathbf{G}^L(\xi,\zeta) = \Big[\underset{(2,2MM)}{\mathbf{G}_I^L(\xi,\zeta)} \ \underset{(2,2MM)}{\mathbf{G}_J^L(\xi,\zeta)} \Big], \mathbf{q}^{L,T} = \Big[\mathbf{q}_I^{L,T} \ \mathbf{q}_J^{L,T} \Big],$$
$$\underset{(2,2MM)}{\mathbf{G}_I^L(\xi,\zeta)} = \begin{bmatrix} N_I F_1 & 0 & N_I F_2 & 0 & N_I F_3 & 0 & N_I F_4 & 0 & \vdots ....\vdots & N_I F_{MM} & 0 \\ 0 & N_I F_1 & 0 & N_I F_2 & 0 & N_I F_3 & 0 & N_I F_4 & \vdots ....\vdots & 0 & N_I F_{MM} \end{bmatrix} =$$
$$= \big[\mathbf{N}_I(\xi) F_1 \ \mathbf{N}_I(\xi) F_2, ..., \mathbf{N}_I(\xi) F_i, ..., \mathbf{N}_I(\xi) F_{MM} \big] \tag{6}$$
$$= \Big[\mathbf{G}_1^I(\xi,\zeta) \ \mathbf{G}_2^I(\xi,\zeta), ..., \mathbf{G}_i^I(\xi,\zeta), ..., \mathbf{G}_{MM}^I(\xi,\zeta) \Big], \quad I \to J$$

and matrices associated with additional constants

$$\underset{(2,2(np-1))}{\hat{\mathbf{G}}_m(\xi,\zeta)} = \begin{bmatrix} N_3 F_m & 0 & N_4 F_m & 0 & \vdots ....\vdots & N_{np} F_m & 0 & N_{np+1} F_m & 0 \\ 0 & N_3 F_m & 0 & N_4 F_m & \vdots ....\vdots & 0 & N_{np} F_m & 0 & N_{np+1} F_m \end{bmatrix}, m = 1, ..., MM \ ,$$
$$\underset{(2,2(np-1)MM)}{\hat{\mathbf{G}}(\xi,\zeta)} = \Big[\hat{\mathbf{G}}_1(\xi,\zeta) \ \hat{\mathbf{G}}_2(\xi,\zeta), ..., \hat{\mathbf{G}}_i(\xi,\zeta), ..., \hat{\mathbf{G}}_{MM}(\xi,\zeta) \Big], \tag{7}$$

furthermore,

$$\mathbf{q}_I^{L,T} = \Big[u^{m=1}, w^{m=1}; u^{m=2}, w^{m=2}; ...; u^{m=i}, w^{m=i}; ...; u^{m=MM}, w^{m=MM} \Big]_I, \quad I \to J \ , \tag{8}$$

$$\underset{(1,2(np-1))}{\hat{\mathbf{a}}^{m,T}} = \left[a_{1r}, a_{1z}; a_{2r}, a_{2z}; ...; a_{ir}, a_{iz}; ..; a_{np-1,r}, a_{np-1,z}; \right]^m, \quad m = 1, ..., MM,$$

$$\underset{(1,2(np-1)MM)}{\hat{\mathbf{a}}^{T}} = \left[\hat{\mathbf{a}}^{m=1,T} \ \hat{\mathbf{a}}^{m=2,T}; ...; \hat{\mathbf{a}}^{m=i,T}; ...; \hat{\mathbf{a}}^{m=MM,T} \right] \quad . \tag{9}$$

Local system derivatives

$$\mathbf{u}_{L,\xi} = \frac{\partial \mathbf{u}_L}{\partial \xi} = \underset{(2,4MM)}{\mathbf{G}^L_{,\xi}(\xi,\zeta)} \underset{(4MM,1)}{\mathbf{q}^L} + \underset{(2,2(np-1)MM)}{\hat{\mathbf{G}}_{,\xi}(\xi,\zeta)} \underset{(2(np-1)MM,1)}{\hat{\mathbf{a}}} \quad , \quad \xi \Rightarrow \zeta \quad , \tag{10}$$

where

$$\mathbf{G}^L_{,\xi} = \mathbf{G}^L_{,\xi}(\xi,\zeta) = \left[\underset{(2,2MM)}{\mathbf{G}^L_{I,\xi}(\xi,\zeta)} \ \underset{(2,2MM)}{\mathbf{G}^L_{J,\xi}(\xi,\zeta)} \right], \quad \xi \Rightarrow \zeta \, , \tag{11}$$

$$\underset{(2,2MM)}{\mathbf{G}^L_{I,\xi}(\xi,\zeta)} = \begin{bmatrix} N_{I,\xi}F_1 & 0 & N_{I,\xi}F_2 & 0 & N_{I,\xi}F_3 & 0 & N_{I,\xi}F_4 & 0 & \vdots \ldots \vdots & N_{I,\xi}F_{MM} & 0 \\ 0 & N_{I,\xi}F_1 & 0 & N_{I,\xi}F_2 & 0 & N_{I,\xi}F_3 & 0 & N_{I,\xi}F_4 & \vdots \ldots \vdots & 0 & N_{I,\xi}F_{MM} \end{bmatrix}, I \to J \, ,$$

$$\underset{(2,2MM)}{\mathbf{G}^L_{I,\zeta}(\xi,\zeta)} = \begin{bmatrix} N_I F_{1,\zeta} & 0 & N_I F_{2,\zeta} & 0 & N_I F_{3,\zeta} & 0 & N_I F_{4,\zeta} & 0 & \vdots \ldots \vdots & N_I F_{MM,\zeta} & 0 \\ 0 & N_I F_{1,\zeta} & 0 & N_I F_{2,\zeta} & 0 & N_I F_{3,\zeta} & 0 & N_I F_{4,\zeta} & \vdots \ldots \vdots & 0 & N_I F_{MM,\zeta} \end{bmatrix}, I \to J \, , \tag{12}$$

$$\underset{(2,2(np-1))}{\hat{\mathbf{G}}_{m,\xi}(\xi,\zeta)} = \begin{bmatrix} N_{3,\xi}F_m & 0 & N_{4,\xi}F_m & 0 & \vdots \ldots \vdots & N_{np,\xi}F_m & 0 & N_{np+1,\xi}F_m & 0 \\ 0 & N_{3,\xi}F_m & 0 & N_{4,\xi}F_m & \vdots \ldots \vdots & 0 & N_{np,\xi}F_m & 0 & N_{np+1,\xi}F_m \end{bmatrix}, m = 1, ..., MM \, ,$$

$$\underset{(2,2(np-1))}{\hat{\mathbf{G}}_{m,\zeta}(\xi,\zeta)} = \begin{bmatrix} N_3 F_{m,\zeta} & 0 & N_4 F_{m,\zeta} & 0 & \vdots \ldots \vdots & N_{np} F_{m,\zeta} & 0 & N_{np+1} F_{m,\zeta} & 0 \\ 0 & N_3 F_{m,\zeta} & 0 & N_4 F_{m,\zeta} & \vdots \ldots \vdots & 0 & N_{np} F_{m,\zeta} & 0 & N_{np+1} F_{m,\zeta} \end{bmatrix}, m = 1, ..., MM \, . \tag{13}$$

From the shape functions under Equation (4) it is seen that the first term under equation (5) describes the linear change of the displacement along the length of the element. From the approximation under Equation (4) it follows that in the I and J nodes the displacement $\mathbf{u}_{L,I} = \sum_{m=1}^{MM} \mathbf{q}_I^{L,m}, I \to J \ \ \mathbf{q}_I^{L,m} = \begin{bmatrix} u \\ w \end{bmatrix}_I^m$ is provided by the summation, since the effect of the term $\hat{\mathbf{G}} \ (\xi,\zeta) \, \hat{\mathbf{a}}$ is zero due to the polynomials under Equation (13). It can be seen that the displacement approximation is formally the same for all m, the difference is carried by the $F_m(\zeta) = (\zeta)^{m-1}$ term. By increasing the hierarchical level of MM, the solution for the shell converges towards the 3D solution. According to the above, our element has two (I and J) nodes for the displacement approximation, see Figure 1b. Furthermore, through the internal parameters we can also provide a higher-order approximation along the length (centerline) of the shell.

Denote the matrix of the transformation between coordinate systems $\mathbf{T}^{LG}$ (from global to local), i.e. the displacement in the global system taking into account $\mathbf{T}^{GL} = \left(\mathbf{T}^{LG}\right)^{-1}$:

$$\mathbf{u}_G = \begin{bmatrix} U(\xi,\zeta) \\ W(\xi,\zeta) \end{bmatrix} = \underset{(2,2)}{\mathbf{T}^{GL}(\xi,\zeta)} \mathbf{u}_L(\xi,\zeta) =$$

$$\underset{(2,2)}{\mathbf{T}^{GL}(\xi,\zeta)} \left\{ \underset{(2,4MM)}{\mathbf{G}^L(\xi,\zeta)} \underset{(4MM,4MM)}{\left\langle \underset{(2,2)}{\mathbf{T}_I^{LG}} \ \mathbf{T}_I^{LG}, ..., \mathbf{T}_J^{LG} \ \mathbf{T}_J^{LG} \right\rangle} \underset{(4MM,1)}{\mathbf{q}^G} + \hat{\mathbf{G}}(\xi,\zeta) \, \hat{\mathbf{a}} \right\},$$

$$
\begin{gathered}
\mathbf{u}_G(\xi,\zeta) = \mathbf{T}^{GL}(\xi,\zeta)\left(\mathbf{G}^L(\xi,\zeta)\mathbf{T}_{IJ}^{LG}\mathbf{q}^G + \hat{\mathbf{G}}(\xi,\zeta)\hat{\mathbf{a}}\right) = \mathbf{G}^G(\xi,\zeta)\mathbf{q}^G + \hat{\mathbf{G}}^G\hat{\mathbf{a}}\,, \\
\mathbf{u}_G = \begin{bmatrix} \mathbf{g}_U^{GT} \\ \mathbf{g}_W^{GT} \end{bmatrix}\mathbf{q}^G + \begin{bmatrix} \hat{\mathbf{g}}_U^{GT} \\ \hat{\mathbf{g}}_W^{GT} \end{bmatrix}\hat{\mathbf{a}}\,, \\
\mathbf{q}_I^{G,T} = \left[U^{m=1}, W^{m=1}; U^{m=2}, W^{m=2}; ...; U^{m=i}, W^{m=i}; ...; U^{m=MM}, W^{m=MM}\right]_I, \quad I \to J\,, \\
\mathbf{q}^{G,T} = \left[\mathbf{q}_I^{G,T}\ \mathbf{q}_J^{G,T}\right], \mathbf{u}_{G,I} = \mathbf{T}^{GL}\mathbf{u}_{L,I}\,.
\end{gathered} \tag{14}
$$

Here $\mathbf{T}_{IJ}^{LG} = \left\langle \underbrace{\mathbf{T}_I^{LG},...,\mathbf{T}_I^{LG}}_{MM},...,\underbrace{\mathbf{T}_J^{LG},...,\mathbf{T}_J^{LG}}_{MM} \right\rangle$ denotes a quasidiagonal matrix, T denotes transpose, $\mathbf{T}_I^{GL}$ is calculated at the node circle I. From the above, it follows that the number of unknown parameters assigned to an element is:
$n_{unknown}^{1\,element} = 4MM + 2(p-1)MM = (4+2(p-1))MM$.

Taking the transformation matrix $\mathbf{T}^{GL}(\xi,\zeta) = \begin{bmatrix} \sin\alpha & \cos\alpha \\ -\cos\alpha & \sin\alpha \end{bmatrix}$ on the midline $r_k = 0.5(r_{1-2} + r_{4-3})$, and taking into account the derivatives by Equation (2) of its elements ($\sin\alpha = z/r_k, \cos\alpha = x/r_k$), we get the following

$$
\begin{gathered}
\sin\alpha_{,\xi} = -\alpha_d \cos(\alpha_k - \xi\alpha_d), \cos\alpha_{,\xi} = +\alpha_d \sin(\alpha_k - \xi\alpha_d)\,, \\
\sin\alpha_{,\zeta} = 0.5b\sin(\alpha_k - \xi\alpha_d)/r_k, \cos\alpha_{,\zeta} = 0.5b\cos(\alpha_k - \xi\alpha_d)/r_k\,.
\end{gathered} \tag{15}
$$

Since $\mathbf{u}_G(\xi,\zeta) = \mathbf{T}^{GL}(\xi,\zeta)\mathbf{u}_L(\xi,\zeta)$, its local system derivatives are

$$
\frac{\partial \mathbf{u}_G(\xi,\zeta)}{\partial \xi} = \frac{\partial \mathbf{T}^{GL}(\xi,\zeta)}{\partial \xi}\mathbf{u}_L(\xi,\zeta) + \mathbf{T}^{GL}(\xi,\zeta)\frac{\partial \mathbf{u}_L(\xi,\zeta)}{\partial \xi} \quad , \xi \Rightarrow \zeta\,. \tag{16}
$$

which is concise

$$
\frac{\partial \mathbf{u}_G(\xi,\zeta)}{\partial \xi} = \begin{bmatrix} \mathbf{g}_{U,\xi}^T \\ \mathbf{g}_{W,\xi}^T \end{bmatrix}\mathbf{q}^G + \begin{bmatrix} \hat{\mathbf{g}}_{U,\xi}^T \\ \hat{\mathbf{g}}_{W,\xi}^T \end{bmatrix}\hat{\mathbf{a}}, \quad \frac{\partial \mathbf{u}_G(\xi,\zeta)}{\partial \zeta} = \begin{bmatrix} \mathbf{g}_{U,\zeta}^T \\ \mathbf{g}_{W,\zeta}^T \end{bmatrix}\mathbf{q}^G + \begin{bmatrix} \hat{\mathbf{g}}_{U,\zeta}^T \\ \hat{\mathbf{g}}_{W,\zeta}^T \end{bmatrix}\hat{\mathbf{a}}\,. \tag{17}
$$

The first members of the resulting vectors correspond to $U_{,\xi}, U_{,\zeta}$ and the second members to $W_{,\xi}, W_{,\zeta}$.

The global derivatives are $U_{,r} = \partial U/\partial r$, $U_{,z} = \partial U/\partial z$ can be calculated using the Jacobian matrix $\mathbf{J}$ [7], that is the global derivatives $\left[U_{,r}\ U_{,z}\ W_{,r}\ W_{,z}\right]$.

$$
\begin{gathered}
\begin{bmatrix} U_{,r} \\ U_{,z} \end{bmatrix} = \mathbf{J}^{-1}\begin{bmatrix} U_{,\xi} \\ U_{,\zeta} \end{bmatrix} = \mathbf{J}^{-1}\left\{\begin{bmatrix} \mathbf{g}_{U,\xi}^T \\ \mathbf{g}_{U,\zeta}^T \end{bmatrix}\mathbf{q}^G + \begin{bmatrix} \hat{\mathbf{g}}_{U,\xi}^T \\ \hat{\mathbf{g}}_{U,\zeta}^T \end{bmatrix}\hat{\mathbf{a}}\right\} = \begin{bmatrix} \mathbf{h}_{U1}^T \\ \mathbf{h}_{U2}^T \end{bmatrix}\mathbf{q}^G + \begin{bmatrix} \hat{\mathbf{h}}_{U1}^T \\ \hat{\mathbf{h}}_{U2}^T \end{bmatrix}\hat{\mathbf{a}}\,, \\
\begin{bmatrix} W_{,r} \\ W_{,z} \end{bmatrix} = \mathbf{J}^{-1}\begin{bmatrix} W_{,\xi} \\ W_{,\zeta} \end{bmatrix} = \mathbf{J}^{-1}\left\{\begin{bmatrix} \mathbf{g}_{W,\xi}^T \\ \mathbf{g}_{W,\zeta}^T \end{bmatrix}\mathbf{q}^G + \begin{bmatrix} \hat{\mathbf{g}}_{W,\xi}^T \\ \hat{\mathbf{g}}_{W,\zeta}^T \end{bmatrix}\hat{\mathbf{a}}\right\} = \begin{bmatrix} \mathbf{h}_{W1}^T \\ \mathbf{h}_{W2}^T \end{bmatrix}\mathbf{q}^G + \begin{bmatrix} \hat{\mathbf{h}}_{W1}^T \\ \hat{\mathbf{h}}_{W2}^T \end{bmatrix}\hat{\mathbf{a}}\,.
\end{gathered} \tag{18}
$$

With the derivatives obtained under Equation (18), the deformation vector for asysimmetric case [7] can be written in the next form

$$\boldsymbol{\varepsilon}=\begin{bmatrix}\varepsilon_r\\ \varepsilon_z\\ \varepsilon_\varphi\\ \gamma_{rz}\end{bmatrix}=\begin{bmatrix}U_{,r}\\ W_{,z}\\ U/r\\ U_{,z}+W_{,r}\end{bmatrix}=\begin{bmatrix}\mathbf{h}_{U1}^T\\ \mathbf{h}_{W2}^T\\ \mathbf{g}_U^{GT}/r\\ \mathbf{h}_{U2}^T+\mathbf{h}_{W1}^T\end{bmatrix}\mathbf{q}^G+\begin{bmatrix}\hat{\mathbf{h}}_{U1}^T\\ \hat{\mathbf{h}}_{W2}^T\\ \hat{\mathbf{g}}_U^{GT}/r\\ \hat{\mathbf{h}}_{U2}^T+\hat{\mathbf{h}}_{W1}^T\end{bmatrix}\hat{\mathbf{a}}=\mathbf{B}(\xi,\zeta)\mathbf{q}^G+\hat{\mathbf{B}}(\xi,\zeta)\hat{\mathbf{a}}$$

(19)

For a homogeneous, isotropic material (E - Young's modulus, ν - Poisson's ratio) the matrix of material constants is:

$$\mathbf{D}=\frac{E}{(1+\nu)(1-2\nu)}\begin{bmatrix}1-\nu & \nu & \nu & 0\\ \nu & 1-\nu & \nu & 0\\ \nu & \nu & 1-\nu & 0\\ 0 & 0 & 0 & \dfrac{1-2\nu}{2}\end{bmatrix}. \qquad (20)$$

The stiffness matrix of the element

$$\mathbf{K}=\int_{-1}^{+1}\int_{-1}^{+1}(\mathbf{B}(\xi,\zeta)\ \hat{\mathbf{B}}(\xi,\zeta))^T\mathbf{D}(\mathbf{B}(\xi,\zeta)\ \hat{\mathbf{B}}(\xi,\zeta))\det\mathbf{J}\ d\xi\ d\zeta\ , \qquad (21)$$

On the surface of radius r_{1-2} from the pressure of intensity p_o

$$\mathbf{f}=\int_{-1}^{+1}(\mathbf{G}^G(\xi,\zeta=-1)\ \hat{\mathbf{G}}^G(\xi,\zeta=-1))^T\mathbf{p}^G 2\pi r\det\mathbf{J}_\Gamma\ d\xi \qquad (22)$$

reduced load vector can be calculated. From the equilibrium equation for the element the parameter $\hat{\mathbf{a}}$ can be eliminated at the elementary level in the usual way [10,17]: $\mathbf{K}_{red}=\mathbf{K}_{qq}-\mathbf{K}_{qa}\mathbf{K}_{aa}^{-1}\mathbf{K}_{aq}$, $\mathbf{f}_{red}=\mathbf{f}_q-\mathbf{K}_{qa}\mathbf{K}_{aa}^{-1}\mathbf{f}_a$, $\hat{\mathbf{a}}=\mathbf{K}_{aa}^{-1}\mathbf{K}_{aq}\mathbf{q}^G+\mathbf{K}_{aa}^{-1}\mathbf{f}_a$.

The elements are coupled with the reduced matrix $\mathbf{K}_{red}$ and the load vector $\mathbf{f}_{red}$ and then after solving the final system of equations, $\hat{\mathbf{a}}$ is calculated element by element. Here $\det\mathbf{J}_\Gamma=r_{1-2}\alpha_d$, $\mathbf{p}^{GT}=p_o\begin{bmatrix}\cos\alpha & \sin\alpha\end{bmatrix}$, $r=r_{1-2}\cos\alpha$.

3 Examples of rotational shells

Let us examine the shell structure, siphon, containing flexible, curved elements, sketched in Figure 2. Elasticity factor: $E=210\,\text{GPa}$, Poisson's ratio: $\nu=0.3$. Load $p_o=5.0$ MPa internal pressure. By changing the angle α_0, we obtain structures with different roundness. $\alpha_0=0$ corresponds to the structure sketched in Figure 2b.

The paper [17] uses thin-shell theory to enable *p*-version calculations. Here, we will perform the calculations with the different hierarchical models ($MM=2,...,8$) described above, or with the ABAQUS or StressCheck program [18,19] using three-dimensional elements. We will also investigate the effect of the shell wall thickness on the accuracy of the models.

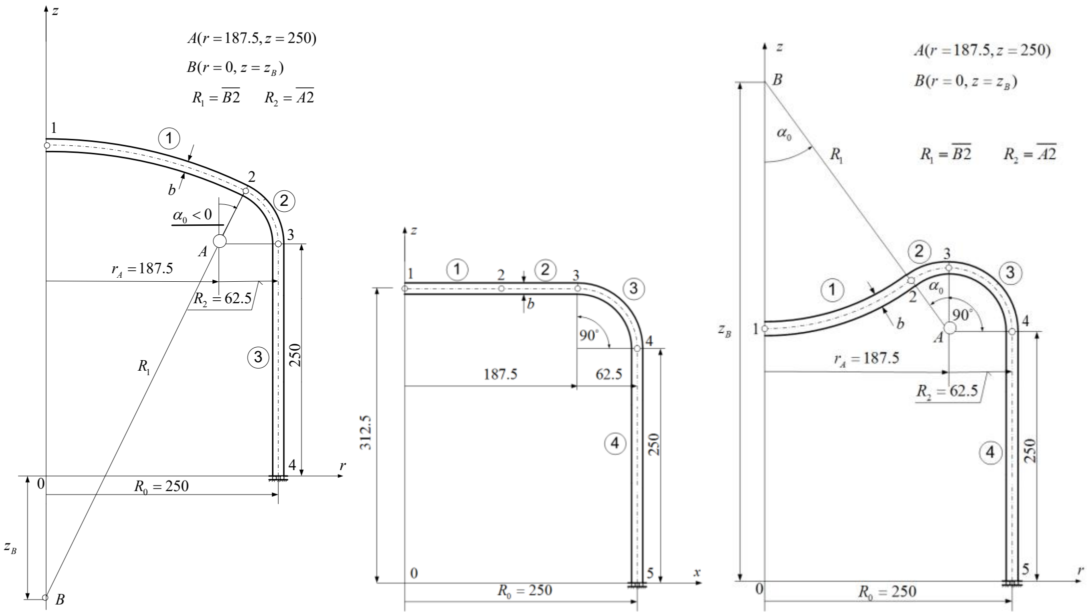

a) b) c)

Figure 2: Diagram underlying the calculation of geometric characteristics belonging to different α_0

For different value of the angle α_0, a fixed radius R_2 has different R_1. This is obtained from simple geometric considerations. We use the fact that the coordinates of point 2 are the same when calculated from circles 1 and 2, i.e.

$r_2 = R_1 \sin\alpha_0 = r_A - R_2 \sin\alpha_0$, $z_2 = z_B - R_1 \cos\alpha_0 = z_A + R_2 \cos\alpha_0$. From here the unknown geometric features $R_1 = \dfrac{r_A}{\sin\alpha_0} - R_2$, $z_B = z_A + (R_1 + R_2)\cos\alpha_0$. In case of negative α_0 $R_1 = -\dfrac{r_A}{\sin\alpha_0} + R_2$, $z_B = z_A - (R_1 - R_2)\cos\alpha_0$.

We use *nel*=13 finite elements for the calculations. At *z*=0, the vertical displacement is zero. In the adopted approximation, we work with polynomials of degree *np*=6 in the longitudinal direction of the elements, while in the transverse direction the approximation is of degree *MM*=8. The wall thickness of the shell can be *b*=20,25,30,35,40 mm. The total number of unknowns is *NEQ* = 14*(2*MM)*, while the number of internal parameters per element is na = 2*(*np*-1)*MM*. This is 10*MM* in the case of *np*=6. At the element level, the internal parameters are eliminated and the algebraic equation system is solved by coupling the obtained reduced stiffness

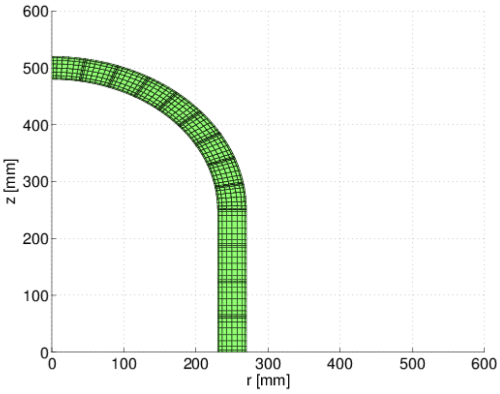

a) $\alpha_0 = -90^\circ$

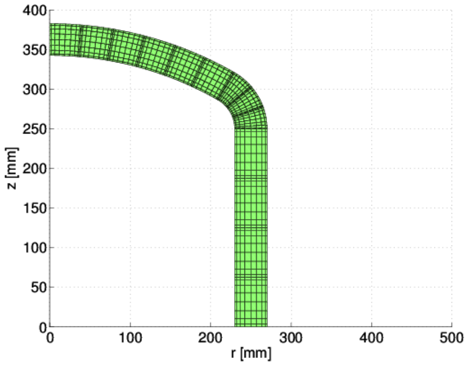

b) $\alpha_0 = -30^\circ$

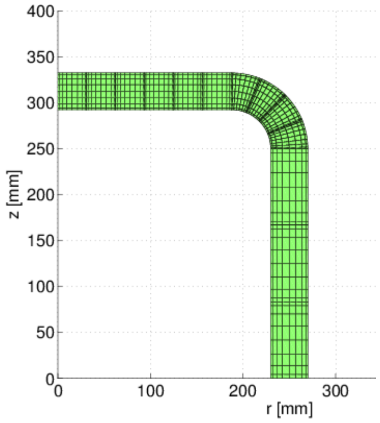

c) $\alpha_0 = 0^\circ$

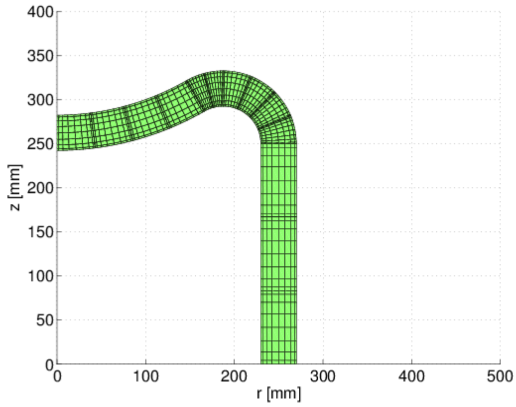

d) $\alpha_0 = 30^\circ$

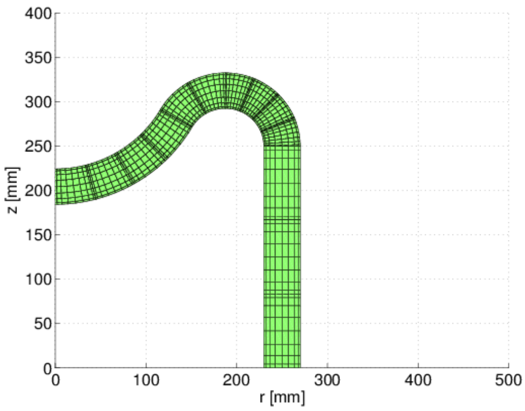

e) $\alpha_0 = 60^\circ$

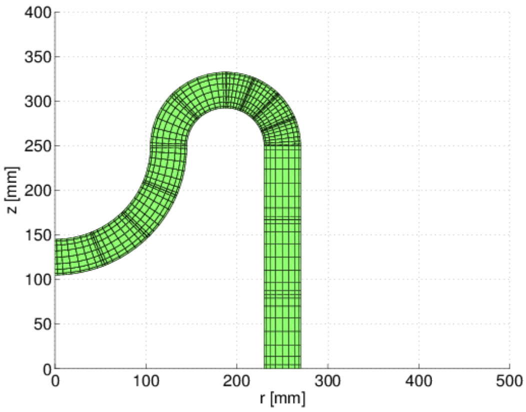

f) $\alpha_0 = 90^\circ$

Figure 3: Siphons with spherical caps of different roundness. The finite element distribution contains 13 elements (the lines correspond to the Lobatto integration lines)

matrices. Knowing the solutions, we calculate the internal parameters as elements and thus the characteristics of the mechanical stress state associated with the task.
The Figure 3 shows shells with a thickness of b=40 mm, choosing different α_0 values. Some of the calculation results are shown in Figure 4.
The volume of the shell structure as a function of α_0 and the wall thickness b is shown in Figure 4a. The changes in the potential energy and the maximum Mises equivalent stress can be seen in Figures 4b, c. Figure 4d shows that the maximum of the equivalent stress on the inner surface reaches its lowest values at 65, 70 degrees at b=30, 40 in the case of α_0 >0.
The equivalent stress characteristics of the solutions vary according to the s coordinate of the shell centerline according to Figure 5 for the points on the inner and outer surfaces of the shell. The ABAQUS solutions for α_0 =0 are also shown

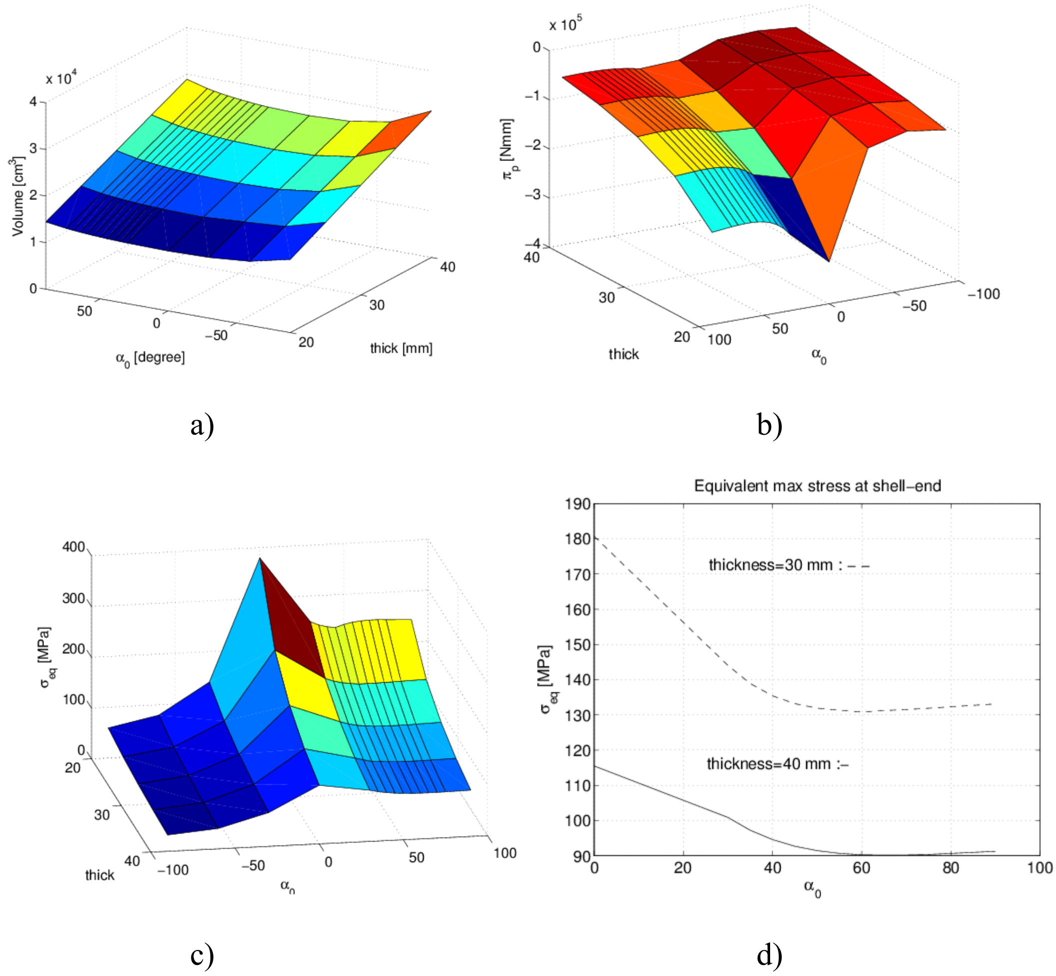

Figure 4: Variation of a) volume, b) potential energy, c) maximum equivalent stress of the siphon ends as a function of α_0 and wall thickness b, d) variation of σ_{eq} in α_0 .

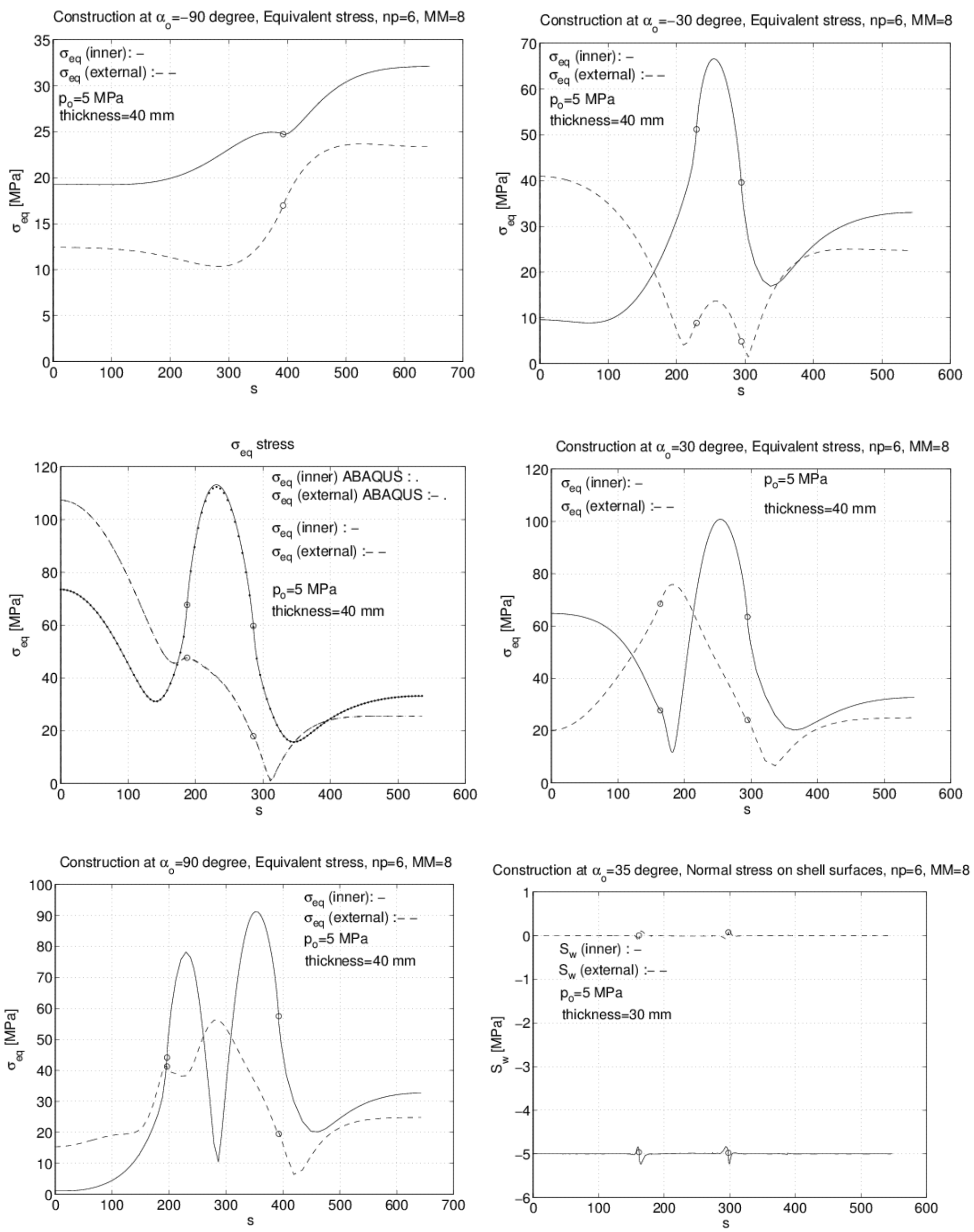

Figure 5: Distribution of equivalent stress σ_{eq}, or $S_w = \sigma_w$ on the inner and outer surfaces of the shell

In the structure according to Figure 2b, the quality of the solution is demonstrated by the fact that on the horizontal section of the bottom $0 \le r \le 187.5$, due to the pressure

p_o, we must have $\sigma_z = -p_o$. This is the case in Figure 6a. Similarly, on the cylindrical section $0 \le z \le 250$, due to the pressure $\sigma_r = -p_o$, see Figure 6b.
The quality of the solution is indicated by the fact that the resultant of σ_z at the I nodal circle of element 11 is 867.453 kN, which is barely different from the vertical resultant of the pressure, 867.472 kN.

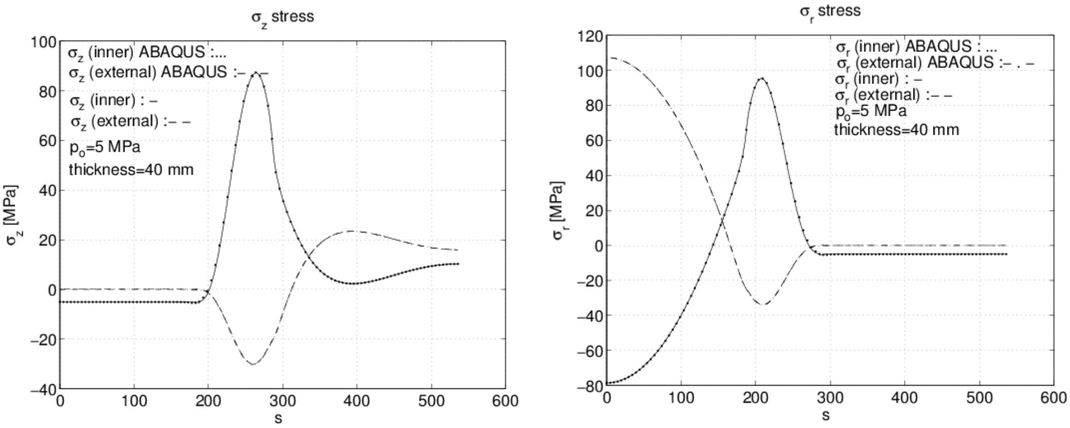

a) b)

Figure 6: σ_z, σ_r stress distribution for the $\alpha_o = 0$ structure

In the range marked by the two circles in Figures 5, the stresses occur at the torus rounding. The peak value of the equivalent stress is redirected to the axis of rotation along the plate section with $\alpha_0 = 0^\circ$ as the wall thickness decreases. In the structure in Figure 2b, the maximum reduced stress at a wall thickness of *b*=20 mm is $\sigma_{eq} \ge \sigma_u = 250\,MPa$, i.e. it exceeds the permissible stress, and the shell enters an elastic-plastic state, which our current model is no longer suitable for determining.
For shells with $\alpha_0 < 0^\circ$, the stresses are lower than for the positive α_0 value. Therefore, if possible, it is more practical to choose $\alpha_0 < 0^\circ$ variants for sealing the cylindrical shell. If the tank has to stand at the sealing part, then the lowest equivalent stresses are achieved at α_0 according to Fig. 4d.
Comparing the structures in Figures 2a, 2b and 2c, it can be stated that the solution for sealing the shell in Figures 2a and 2c is more favorable than the cylindrical container closed with a flat bottom.
The convergence of the solution to the structure of Fig. 2c (*b*=30) is shown in Fig. 7. It is clear from these that the values over *np*=4 and *MM*=6 hardly change. Since at *r*=0 the inner surface point of the shell $\sigma_z = -p_o = -5$MPa is the required value, we can evaluate the error of the obtained solutions compared to the exact solution. At *np*=4, *MM*=6 the error of the deviation is 0.123%, while at *np*=6, *MM*=8 it is -0.04%. The potential energy in the $np \le 5, MM \le 6$ interval remains constant.

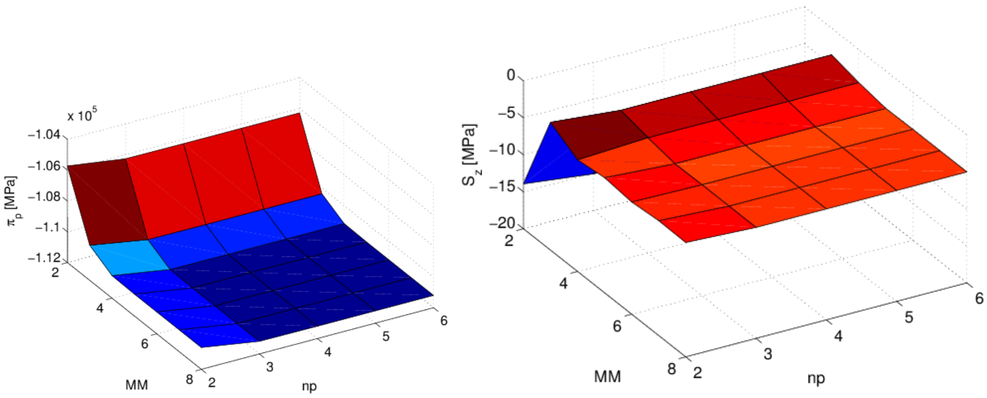

a) b)

Figure 7. Convergence surfaces: a) Π_p potential energy, b) $S_z = \sigma_z(r = 0, z = 238.38)$.

4 Conclusions

Solving the presented examples with hierarchical models convincingly demonstrated that convergent solutions can be achieved with a sufficient number of elements and hierarchical levels. Applying the principle of minimum potential energy enabled the determination of stress boundary conditions with high accuracy, ensuring global equilibrium. By choosing variable *MM* and *np* in the solution of the problem, the situations where classical shell theories can still be applied due to the polynomial order of the approximating fields, or where their application can be considered ineffective, became clear. Here, the *MM* provides the basis for deciding whether the theories are comparable. The rate of change of the thickness displacement, whether constant, linear, quadratic, etc., provides the answer to this question.

With suitable design of the computer program, it is possible to perform calculations with different *MM* values during one run, i.e. to check convergence, and thus decide whether our solution has the desired accuracy or whether further model improvement is necessary. The correctness of our developed model is also proven by the fact that our results have a small difference compared to other finite element (ABAQUS program using 3D elements) calculations, meaning we can speak of a good approximation.

Overall, we can say that the proposed hierarchical shell model gives good results with few unknowns.

Acknowledgement

The present research was partially supported by the Hungarian Academy of Sciences

References

[1] L. Euler, ”De curvis elasticis, In: Methodus inveniendi lineas curvas maximi minimive proprietate gaudentes, Sive solutio problematis isopermetrici lattissimo sensu accepti”, Bousquet, 1744.
[2] S.P. Timoshenko, ”On the corrections for shear of the differential equation for transverse vibrations of prismatic bars”, Philosophical Magazine, 41, 744-746, 1921.
[3] S.P. Timoshenko, S. Woinowsky-Krieger, „Theory of plates and shells”, McGraw-Hill, New York, 1959.
[4] E. Reissner, “The effect of transverse shear deformation on the bending of elastic plates”, ASME Journal of Applied Mechanics, Vol. 12, A68–77, 1945.
[5] R. D. Mindlin, “Influence of rotatory inertia and shear on flexural motions of isotropic, elastic plates”, ASME Journal of Applied Mechanics, Vol. 18, 31–38, 1951.
[6] P.M. Naghdi, ”The Theory of Shells and Plates”. Handbuch der Physik, vol. VIa/2, 425–640. Springer, New York,1972.
[7] J.N. Reddy, ”Theory and analysis of elastic plates and shells”, CRC Press, Boca Raton, FL, 2007.
[8] J.N. Reddy, ”A general non-linear third-order theor of plates with moderate thickness”, Journal of non-linear mechanics, 25, 677-686, 1990.
[9] B. Szabó, G. J. Sahrmann: ”Hierarchic plate and shell models based on p-extension*”*, Int. J. numer methods eng., 26, 1855-1881, 1988. https://doi.org/10.1002/nme.1620260812
[10] B. Szabó, I. Babuska, ”Introduction to Finite Element Analysis: Formulation, Verification and Validation”, John Wiley and Sons, Ltd, Chichester, UK, 2011.
[11] I. Páczelt, B. Szabó, A. Baksa, ”Application of the p-version of FEM to hierarchic rod models with reference to mechanical contact problems*”*, Journal of Computational and Applied Mechanics, 18, No1, 35-84, 2023.
DOI: 10.32973/jcam.2023.002
[12] E. Carrera, G. Giunta, M. Petrolo, ”Beam structures, Classical and advanced theoris”, John Wiley and Sons, Ltd, 2011.
[13] E. Rank, A. Düster, V. Nübel, K. Preusch, O.T. Bruhns, ”Higher order finite elements for shells*”*. Comput. Methods Appl. Mech. Eng.194, 2494–2512, 2005. https://doi.org/10.1016/j.cma.2004.07.042
[14] J. Freund, ”Shear-corrected Reissner–Mindlin plate mo*del”*. Compos. Struct. 211,144–153, 2018.. https://doi.org/10.1016/j.compstruct.2018.12.029
[15] M.L. Bucalem, K-J. Bathe, ”The mechanics of solids and structures- hierarchical modeling and the finite element solution”, Springer, Heidelberg, New York, 2011.
[16] S.P. Timoshenko, J.N. Goodier, ”Theory of elasticity”, McGraw-Hill, London, 1970.
[17] B. Herpai, I. Páczelt: ”Analysis of axisymmetrically deformed shells by the finite element displacement methods*”*. Acta Techn. Hung. 85, 93-122, 1977.
[18] Abaqus, http://www.abaqus.com
[19] StressCheck, https://esrd.com